Topological transition in measurement-induced geometric phases

Valentin Gebhart[a,b,1], **Kyrylo Snizhko**[b,1], **Thomas Wellens**[a], **Andreas Buchleitner**[a], **Alessandro Romito**[c], **and Yuval Gefen**[b,2]

[a]Physikalisches Institut, Albert-Ludwigs-Universität Freiburg, Hermann-Herder-Str. 3, 79104 Freiburg, Federal Republic of Germany; [b]Department of Condensed Matter Physics, Weizmann Institute of Science, Rehovot 76100, Israel; [c]Department of Physics, Lancaster University, Lancaster LA1 4YB, United Kingdom

This manuscript was compiled on March 4, 2020

The state of a quantum system, adiabatically driven in a cycle, may acquire a measurable phase depending only on the closed trajectory in parameter space. Such geometric phases are ubiquitous, and also underline the physics of robust topological phenomena such as the quantum Hall effect. Equivalently, a geometric phase may be induced through a cyclic sequence of quantum measurements. We show that the application of a sequence of weak measurements renders the closed trajectories, hence the geometric phase, stochastic. We study the concomitant probability distribution and show that, when varying the measurement strength, the mapping between the measurement sequence and the geometric phase undergoes a topological transition. Our finding may impact measurement-induced control and manipulation of quantum states—a promising approach to quantum information processing. It also has repercussions on understanding the foundations of quantum measurement.

Quantum measurement | quantum trajectories | quantum feedback | Berry phase | topological phases of matter

The overall phase of a system's quantum state is an unmeasurable quantity that can be freely assigned. However, when the system is driven slowly in a cycle, it undergoes an adiabatic evolution which may bring its final state back to the initial one (1, 2); the *accumulated* phase then becomes gauge invariant and, therefore, detectable. As noted by Berry (3), this is a geometric phase (GP) in the sense that it depends on features of the closed trajectory in parameter space, and not on the dynamics of the process. Geometric phases are key to understanding numerous physical effects (4–6), enabling the identification of topological invariants for quantum Hall phases (7), topological insulators and superconductors (8, 9), defining fractional statistics anyonic quasiparticles (10, 11), and opening up applications to quantum information processing (12, 13).

Geometric phases are not necessarily a consequence of adiabatic time evolution. For any pair of states $|\psi_l\rangle$,$|\psi_m\rangle$ in Hilbert space, it is possible to define a relative phase, $\chi_{l,m} \equiv \arg\left[\langle\psi_l|\psi_m\rangle\right]$. For a sequence of states (14, 15) $|\psi_k\rangle$, $k = 0,\dots,N$, for which $|\psi_N\rangle \propto |\psi_0\rangle$, one can define the total phase accumulated through the sequence (the Pancharatam phase (14, 15))

$$\chi^{(P)}_{\rm geom} = \sum_{k=0}^{N-1} \chi_{k+1,k} = \arg\left[\langle\psi_0|\,\mathcal{P}_N\dots\mathcal{P}_2\mathcal{P}_1\,|\psi_0\rangle\right] = \arg\langle\psi_0|\tilde{\psi}_N\rangle, \quad [1]$$

where $|\tilde{\psi}_k\rangle = \mathcal{P}_k\dots\mathcal{P}_2\mathcal{P}_1|\psi_0\rangle$ and $\mathcal{P}_k = |\psi_k\rangle\langle\psi_k|$ is the projector onto the k-th state. Note that $|\tilde{\psi}_k\rangle \propto |\psi_k\rangle$ is not normalized, which however does not undermine the definition of the phase (unless some $|\tilde{\psi}_k\rangle = 0$). Note also that $\chi^{(P)}_{\rm geom}$ is independent of the gauge choice of phases of all $|\psi_k\rangle$. For a quasicontinuous sequence of states $\{|\psi_k\rangle\}$, the Pancharatnam phase trivially coincides with the Berry phase under the corresponding continuous state evolution. Moreover, for *any* sequence $\{|\psi_k\rangle\}$, the Pancharatnam phase is equal to the Berry phase associated with the trajectory that connects the states $|\psi_k\rangle$ by the shortest geodesics in Hilbert space (6, 16).

The Pancharatam phase can quite naturally be interpreted as a result of a sequence of strong (projective) measurements acting on the system and yielding specific measurement readouts (17). This interpretation is valid for optical experiments observing the Pancharatnam phase induced with sequences of polarizers (18). Such a phase can be consistently defined despite the fact that measurements (typically considered an incoherent process) are involved. A generic sequence of measurements is an inherently stochastic process. One thus expects a distribution of measurement-induced geometric phases, determined by the sequences of measurement readouts associated with the corresponding probabilities. For a quasicontinuous sequence of strong measurements ($N \to \infty$ and $\||\psi_{k+1}\rangle - |\psi_k\rangle\| = O(1/N)$), the induced evolution is fully deterministic due to the dynamical quantum Zeno effect (17), thus yielding a unique Pancharatnam-Berry phase.

Recently, geometric phases induced by *weak measurements* (that do not entirely collapse the system onto an eigenstate of the measured observable (19)) have been experimentally observed (20). The setup of Ref. (20) ensured that only one possible readout sequence contributed to the observed phase. When considering all possible readout sequences, the system dynam-

Significance Statement

We bring together two concepts at the forefront of current research: measurement-induced back-action (resulting in the steering of a quantum state), and topological transitions. It has been widely believed that the transition from the limit of a strong (projective) measurement to that of weak measurement involves a smooth crossover as function of the measurement strength. Here we find that varying the measurement strength continuously may involve a topological transition. Specifically, we address measurement-induced geometric phase, which emerges following a cyclic sequence of measurements. Our analysis suggests that measurement-based control and manipulations of quantum states (a promising class of quantum information protocols) may involve subtle topological features that have not been previously appreciated.

The authors declare no conflict of interest.

[1]V.G. and K.S. contributed equally to this work.

[2]E-mail: yuval.gefen@weizmann.ac.il

ics remains stochastic even for quasicontinuous sequences of weak measurements (21, 22). In a wider context, employing weak measurements enables continuous monitoring of the system through weak measurements, which has been successfully employed experimentally for dynamically controlling quantum states (23–26).

In the present study, we define and investigate the geometric phase accrued by a quantum state of a two-level system following a sequence of measurements and detector readouts with tunable measurement strength. We compute the full distribution function of the induced geometric phases and analyze the phase of specific trajectories which can be singled out by postselecting specific readout sequences. As opposed to the case of projective measurements (17, 18), where the state trajectory (and the resulting phase) are solely determined by the measurement sequence and the measurement readouts, the trajectories (and the phases) here depend crucially on the measurement strength. We mainly focus on the scenarios of a single postselected state trajectory and consider the effect of averaging over all possible trajectories in the Supplementary Material.

We discover that a topological transition vis-à-vis the geometric phase takes place as a function of the measurement strength. The transition is topological in the sense that it is related to a discontinuous jump of an integer-valued topological invariant. Specifically, we consider a family of measurement sequences: The state trajectories induced by these sequences form a surface which covers a certain area on the Bloch sphere, and our topological transition is manifest through a jump of the Chern number associated with this surface. Finally, we propose concrete interferometry protocols, which allow us to consistently define geometric phases in the presence of detectors, and facilitate their detection.

Defining geometric phases from variable strength quantum measurements

Our system is a qubit whose Hilbert space is spanned by $|\uparrow\rangle, |\downarrow\rangle$. The system undergoes a chronological sequence of weak measurements, labeled as $k = 1, \ldots, N$. The measured observables are represented by the operators $\sigma_{\mathbf{n}_k} = \boldsymbol{\sigma} \cdot \mathbf{n}_k$, where $\boldsymbol{\sigma} = (\sigma_x, \sigma_y, \sigma_z)$ is the vector of Pauli matrices and $\mathbf{n}_k = (\sin\theta_k \cos\varphi_k, \sin\theta_k \sin\varphi_k, \cos\theta_k)$. The sequence of measurement orientations $\{\mathbf{n}_k\}$ defines a trajectory on the unit sphere S^2 as depicted in Fig. 1 (left). Each weak measurement is characterized by its strength $\eta \in [0, 1]$ and two possible readouts $r_k = +, -$. The modification of the system state conditional to the obtained measurement readout r_k is given by $|\psi\rangle \to \mathcal{M}_k^{(r_k)}|\psi\rangle$, where $\mathcal{M}_k^{(r_k)} = M_{\eta_k}(\mathbf{n}_k, r_k)$ are Kraus operators (21, 22) (cf. Methods below). Given the measurement strength η, a sequence $\{\mathbf{n}_k\}$ of measurement orientations with corresponding readouts $\{r_k\}$ induces a sequence of states $\left\{|\tilde{\psi}_k\rangle\right\}$ in the system Hilbert space, where

$$|\tilde{\psi}_k\rangle = |\tilde{\psi}_{r_1,\ldots,r_k}\rangle = \mathcal{M}_k^{(r_k)} \ldots \mathcal{M}_1^{(r_1)} |\psi_0\rangle \,. \qquad [2]$$

The weak measurement-induced geometric phase can be defined as

$$\chi_{\text{geom}} = \arg\langle\psi_0|\tilde{\psi}_N\rangle = \arg\langle\psi_0| \mathcal{M}_N^{(r_N)} \ldots \mathcal{M}_1^{(r_1)} |\psi_0\rangle \,. \qquad [3]$$

In order to further proceed with our analysis we need to specify the nature of the measurement. For the present study we opt for so-called null-type weak measurements (27–29). The state before the measurement is $|\psi\rangle = a|\mathbf{n}\rangle + b|-\mathbf{n}\rangle$, where $\sigma_{\mathbf{n}}|\pm\mathbf{n}\rangle = \pm|\pm\mathbf{n}\rangle$, while the detector initial state is $|+\rangle$. The measurement process is mediated by the system-detector interaction which is described by the interaction-induced mapping

$$\begin{aligned}(a|\mathbf{n}\rangle + b|-\mathbf{n}\rangle)|+\rangle \\ \to \left(a|\mathbf{n}\rangle + b\sqrt{1-\eta}|-\mathbf{n}\rangle\right)|+\rangle + b\sqrt{\eta}|-\mathbf{n}\rangle|-\rangle \,. \qquad [4]\end{aligned}$$

Following this step, the detector is projectively measured in the basis of $|\pm\rangle$ states. Note that this measurement protocol has the following properties: (i) if the initial system state is $|\mathbf{n}\rangle$ ($a = 1$, $b = 0$ in Eq. (4)), it gives with certainty readout $r = +$ and does not alter the state of the system; (ii) if the initial system state is $|-\mathbf{n}\rangle$ ($a = 0$, $b = 1$ in Eq. (4)), it yields readouts $r = -$ or $r = +$ with probabilities $p_- = \eta$ and $p_+ = 1-\eta$, respectively, again without altering the state of the system. In general, when the system state is in a superposition of $|\mathbf{n}\rangle$ and $|-\mathbf{n}\rangle$, the measurement *does* alter the system state. For $\eta \ll 1$, the detector remains practically always in its initially prepared state ($r = +$, i.e., null-outcome), modifying the system state only slightly; yet with probability $\eta|b|^2$ the readout is $r = -$, inducing a jump in the system state to $|-\mathbf{n}\rangle$. Considering only the experimental runs resulting in $r = +$ allows one to define "null weak values" (27, 28). For arbitrary η, such postselected measurements may be implemented, with imperfect polarizers, as depicted in Fig. 2: a photon of one polarization is always transmitted ($r = +$), while a photon of the orthogonal polarization has finite probability to be transmitted ($r = +$) or absorbed ($r = -$). Here, we do not restrict ourselves to postselected measurements and to the $\eta \ll 1$ limit. Below (cf. Methods) we address a Hamiltonian implementation of such measurements in the spirit of the von Neumann (30) measurement model.

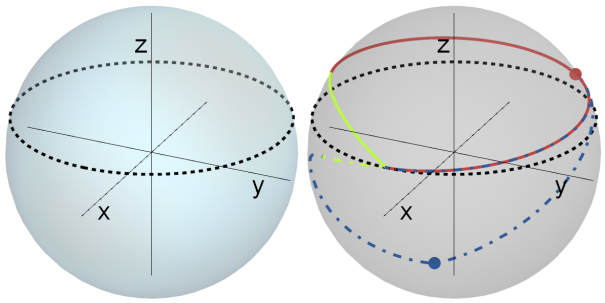

Fig. 1. Measurement sequences and induced quantum trajectories. (left) A measurement sequence spanned by the directions $\mathbf{n}_k = (x_k, y_k, z_k) = (\sin\theta_k\cos\varphi_k, \sin\theta_k\sin\varphi_k, \cos\theta_k)$, following a parallel ($\theta_k = \pi/4$ and $\varphi_k = 2\pi k/N$). (right) Quantum trajectories on the Bloch sphere induced by the measurement sequence depicted on the left for different measurement strengths and readout sequences. The trajectory induced by the $\{r_k = +\}$ readout sequence for strong measurements ($c = +\infty$, dotted black) meticulously follows the measurement eigenstates $|+\mathbf{n}_k\rangle$, while the $\{r_k = +\}$ trajectory for finite-strength measurements ($c = 3$, red) deviates from this line. A weak-measurement-induced trajectory ($c = 3$) corresponding to the readout sequence with all $r_k = +$ except for a single $r_{k_0} = -$ readout is depicted by the dot-dashed (blue) line. The "$-$" readout induces a state jump from its position on the red line (red dot) to the blue dot via the shortest geodesic on the Bloch sphere. For weak measurements, the quantum trajectory does not coincide with the measurement sequence and may not terminate at the initial state (red and blue lines). The final measurement (yellow segment) projects the N-th state onto the initial state via the shortest geodesic.

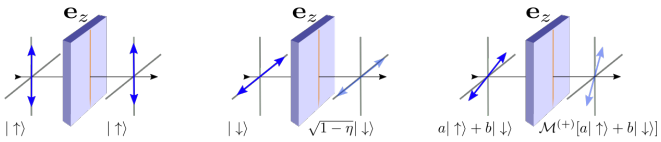

Fig. 2. An imperfect polarizer implementing a null-type weak measurement. Each polarizer transmits a certain polarization (here, $\mathbf{e}_z$), with certainty. An impinging beam with generic polarization (blue arrows) is either transmitted, resulting in a null readout, $r = +$, or absorbed, $r = -$. (a) A vertically polarized photon ($|\uparrow\rangle$) is transmitted without altering its polarization; (b) a horizontally polarized photon ($|\downarrow\rangle$) is transmitted with a probability 1-$\eta < 1$ (pale blue arrow); (c) a photon of generic polarization $|\psi\rangle = a\,|\uparrow\rangle + b\,|\downarrow\rangle$ is transmitted with probability $|a|^2 + (1-\eta)\,|b|^2$ and a modified polarization state , $|\psi\rangle \to M_\eta(\mathbf{e}_z, r = +)|\psi\rangle = \mathcal{M}^{(+)}\,|\psi\rangle$. By rotating the polarizers and adding phase plates (e.g., quarter-wave plates), it is possible to engineer a fully transmitted polarization direction $|+\mathbf{n}\rangle = \cos\theta/2\,|\uparrow\rangle + e^{i\varphi}\sin\theta/2\,|\downarrow\rangle$.

Define the normalized state $|\psi_k\rangle = |\tilde{\psi}_k\rangle/\sqrt{\langle\tilde{\psi}_k|\tilde{\psi}_k\rangle}$. With the standard parametrization, $|\psi_k\rangle = e^{i\alpha_k}(\cos\Theta_k/2\,|\uparrow\rangle + e^{i\Phi_k}\sin\Theta_k/2\,|\downarrow\rangle)$, the sequence of states is mapped onto a discrete trajectory on the Bloch sphere with spherical coordinates Θ_k and Φ_k. Fig. 1(right) depicts state trajectories that correspond to measurement orientation sequences (Fig. 1(left)) of various measurement strengths. The particular type of measurement we employ guarantees that $\langle\tilde{\psi}_k|\tilde{\psi}_{k-1}\rangle = \langle\tilde{\psi}_{k-1}|\,\mathcal{M}_k^{(r_k)\dagger}\,|\tilde{\psi}_{k-1}\rangle = \left(\langle\tilde{\psi}_{k-1}|\,\mathcal{M}_k^{(r_k)}\,|\tilde{\psi}_{k-1}\rangle\right)^* > 0$, enabling us to express the above geometric phase in the same form as the Pancharatnam phase (1). It thus follows that $\chi_{\rm geom} = -\Omega/2$ can be expressed via the solid angle Ω subtended by a piecewise trajectory on the Bloch sphere that connects the neighboring states ($|\psi_k\rangle$ and $|\psi_{k+1}\rangle$; here we imply $|\psi_{N+1}\rangle \coloneqq |\psi_0\rangle$) along shortest geodesics. Note the difference between weak and projective measurements. In the latter, the system states $|\psi_k\rangle$ are fully determined by the measurement orientation and the measurement readout r_k. By contrast, the system state following a weak measurement also depends on its strength $\eta < 1$ and on the state before the measurement. Furthermore, for a quasicontinuous sequence of strong measurements ($N \to \infty$ and $\|\mathbf{n}_{k+1} - \mathbf{n}_k\| = O(1/N)$), the readout $r_k = -$ is impossible due to the dynamical quantum Zeno effect (17), rendering all readouts $r_k = +$ and the measurement-induced trajectory deterministic. For a quasicontinuous sequence of *weak* measurements, the trajectory is, instead, stochastic, manifested in a variety of possible readout sequences $\{r_k\}$, cf. Fig. 1(right). The probability of obtaining a specific sequence of readouts $\{r_k\}$ is given by $P_{\{r_k\}} = \langle\tilde{\psi}_N|\tilde{\psi}_N\rangle$.

For a general choice of η the final state $|\tilde{\psi}_N\rangle$ may not be proportional to the initial state $|\psi_0\rangle$, meaning the trajectory $|\psi_1\rangle \to \ldots \to |\psi_N\rangle$ is not closed. For simplicity, we take the last measurement to be strong ($\eta_N = 1$) and *postselect* it to yield $r_N = +$ (i.e., discard those experimental runs that yield $r_N = -$), hence $\mathcal{M}_N^{(r_N)} = \mathcal{M}_N^{(+)} = |\psi_0\rangle\langle\psi_0| = \mathcal{P}_0$. The probability of getting a specific sequence of readouts $\{r_k\}$ can then be expressed as

$$P_{\{r_k, r_N=+\}} = \left|\langle\psi_0|\tilde{\psi}_N\rangle\right|^2 = \left|\langle\psi_0|\tilde{\psi}_{N-1}\rangle\right|^2 \qquad [5]$$

with $\left|\tilde{\psi}_N\right\rangle = \left|\tilde{\psi}_{\{r_k\}}\right\rangle$ as defined in Eq. (2). Thus,

$$\langle\psi_0|\,\mathcal{M}_{N-1}^{(r_{N-1})}\ldots\mathcal{M}_1^{(r_1)}\,|\psi_0\rangle = \sqrt{P_{\{r_k, r_N=+\}}}\,e^{i\chi_{\rm geom}}. \qquad [6]$$

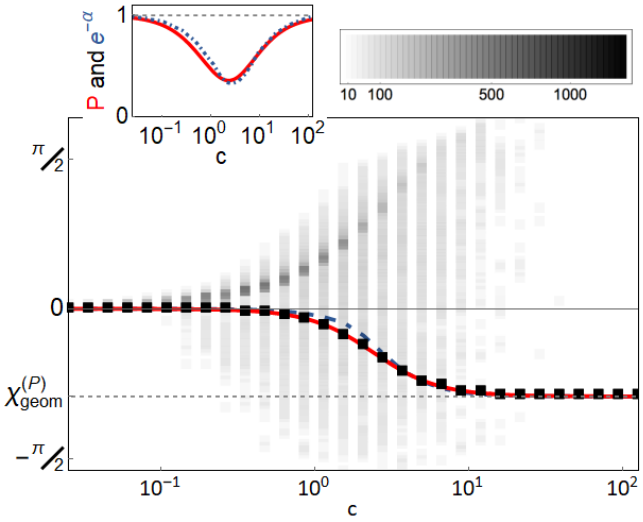

Fig. 3. Statistics of the measurement induced geometric phase. The geometric phase induced by continuous measurements ($\theta = \pi/4$) as a function of the parameter c controlling the strength of measurements: For the $\{r_k = +\}$ postselected trajectory, $\chi_{\rm geom}$ is given by Eq. (7) (red solid line). The averaged geometric phase, $\bar{\chi}_{\rm geom}$ Eq. (8), is represented by the blue dot-dashed line. Both curves show a similar transition from a finite geometric phase for strong measurements to a vanishing one in the weak measurement limit. The gray-scale density plot shows the probability distribution of the geometric phases in the absence of postselection. Note that the phase of the postselected trajectory is the most probable one (black squares). For $c \simeq 0.1 \ldots 1$, a secondary peak emerges, and persists for intermediate measurement strengths before fading out again. In the weak measurement regime, the $r_k = -$ readouts are not probable due to the weakness of the measurement. The secondary peak seems to arise due to the trajectories with a single $r_k = -$ readout at $k \sim N/2$, where the probability of such a readout is the highest. At intermediate measurement strengths, the distribution is dichotomic and broader as the probability of $r_k = -$ outcomes is higher. For large c, the secondary peak is suppressed and the distribution finally collapses onto the result enforced by the dynamical quantum Zeno effect. Inset: The probability of observing the $\{r_k = +\}$ readout sequence (red solid line) and the suppression factor $e^{-\alpha}$ in Eq. (8) (blue dot-dashed line) arising due to averaging ($\theta = \pi/4$). The probability distribution and averaging were obtained performing Monte Carlo simulations with $N = 500$ measurements per sequence and $N_{\rm realizations} = 4000$ realizations.

We next study $\chi_{\rm geom}$ as a function of the measurement strength. We consider $N \to \infty$ measurements with measurement orientations $\{\mathbf{n}_k\}$ that follow a given parallel on the sphere, $(\theta_k, \varphi_k) = (\theta, 2\pi k/N)$. The initial state is $|\psi_0\rangle = \cos\theta/2\,|\uparrow\rangle + \sin\theta/2\,|\downarrow\rangle$, cf. Fig. 1(right). The measurement strength of each individual measurement is $\eta_k = \eta = 4c/N \to 0$ with c being a non-negative constant (except for $\eta_N = 1$). The sequence of $N-1$ weak measurements can be characterized by an effective measurement strength $\eta_{\rm eff} = 1 - e^{-4c}$, $0 \leqslant \eta_{\rm eff} \leqslant 1$.

Probability distribution of the measurement-induced geometric phase

The probability distribution of the geometric phases is reported in Fig. 3 as a function of the parameter c quantifying the effective measurement strength. For $c \to 0$, the distribution is peaked around $\chi_{\rm geom} = 0$ corresponding to a vanishing backaction from the measurement process. With increasing measurement strength, the distribution develops a main peak which continuously evolves towards the Pachnaratnam phase in the strong measurement limit. This peak corresponds to the the most probable trajectory associated with a specific readout sequence, $r_k = +$ for all k, cf. Fig. 1 (red solid line).

A secondary peak develops for intermediate measurement strengths due to the non-vanishing probability of obtaining $r_k = -$ for some k.

We first turn our attention to the geometric phase associated with a specific readout sequence, $r_k = +$ for all k (this means that if any $r_k = -$, that particular experimental run should be discarded). For a generic measurement strength, it is the most probable measurement outcome, hence the corresponding GP is the most likely one. We parametrize the Hilbert space trajectory as $|\psi(t)\rangle$, $t \in [0, 2\pi]$, so that $|\psi(t = \pi k/N)\rangle = |\psi_k\rangle$ for $k = 1, ..., N-1$ and $|\psi(t \in [\pi, 2\pi])\rangle$ is the shortest Bloch sphere geodesic between $|\psi_{N-1}\rangle$ and $|\psi_N\rangle = |\psi_0\rangle$, cf. Fig. 1(right). This parametrization results in a quasi-continuous trajectory since $\||\psi_{k+1}\rangle - |\psi_k\rangle\| = \mathcal{O}(1/N)$ for $k < N-1$. We investigate the behavior of $\chi_{\rm geom}$ and link it to the behavior of $|\psi(t)\rangle$ as a function of the measurement strength η. Since the measurements are not projective (measurement strength $\eta \to 0$), the state after each measurement is not necessarily the $\uparrow$-eigenstate of $\sigma_{\mathbf{n}_k}$. The state trajectory on the Bloch sphere for $\theta = \pi/4$ and $c = 3$ is shown in Fig. 1 (red solid line). The probability $P = P_{\{r_k=+\}}$ of measuring the desired readouts and the corresponding geometric phase $\chi_{\rm geom}$ (cf. Eq. (6)) can be calculated analytically for $N \to \infty$ and are given by

$$\sqrt{P} e^{i\chi_{\rm geom}} = -e^{-c}(\cosh(\tau) + z \sinh(\tau)/\tau), \qquad [7]$$

with $\tau = \sqrt{z^2 - \pi^2 \sin^2\theta}$ and $z = c + i\pi\cos\theta$, cf. Fig. 3 (red solid lines).

We note three qualitatively different regimes depending on the parameter c controlling the effective measurement strength. For strong measurements ($c \to \infty$), one obtains Zeno-like dynamics: the state follows meticulously the measurement orientation. In this limit, the probability of the successful postselection of the measurement readouts approaches 1 and the GP is $-\Omega/2$: half the solid angle enclosed by the measurement orientation, $\Omega = 2\pi(1 - \cos\theta)$. Similarly, in the infinitely weak measurement limit ($c \to 0$), the probability of obtaining all readouts $r_k = +$ approaches 1. In this limit, however, the result stems from the fact that the system barely interacts with the detector (cf. Eq. (4)); $r_k = +$ is the only possible measurement readout and back-action is practically absent: the system remains in its initial state at all times and accumulates no geometric phase. Finally, for intermediate strength measurements, the system reacts to the measurement, yet its state does not follow the measurement orientation but has a readout-sequence-dependent non-trivial trajectory. As a consequence, the trajectory with all readouts $r_k = +$ occurs with reduced probability and a smaller postselected geometric phase as compared with the strong measurement limit.

As a follow up, we characterize the effect of the probability distribution of $\chi_{\rm geom}$ by studying the average GP and its behavior as a function of η. We define the averaged geometric phase $\bar{\chi}_{\rm geom}$ as

$$e^{2i\bar{\chi}_{\rm geom} - \alpha} := \langle e^{2i\chi_{\rm geom}} \rangle_{\rm realizations} = \sum_{\{r_k\}} \left(\langle\psi_0| \mathcal{M}_{N-1}^{(r_{N-1})} \dots \mathcal{M}_1^{(r_1)} |\psi_0\rangle \right)^2, \qquad [8]$$

motivated by physically measurable observables (cf. Supplementary Material). Here, the sum extends over all possible measurement readouts $\{r_k\}$. Also for the averaged phase,

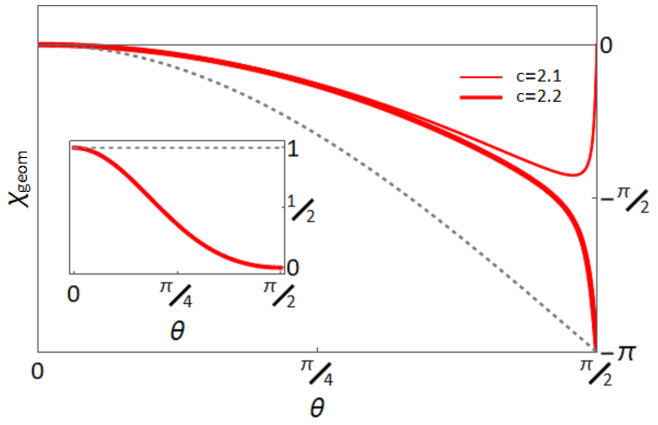

Fig. 4. Non-monotonicity of geometric phases. Dependence of the geometric phase on the polar angle θ for the postselected trajectory (red solid lines) for different values of the integrated measurement strength (cf. legend). The ideal strong measurement dependence for $c \to \infty$ is presented as a grey dashed line. The asymptotic dependence of the GP on θ displays an abrupt transition from monotonic to non-monotonic behavior in the vicinity of $c = 2.15$. The behavior is underlined by the fact that $\chi_{\rm geom}(\pi/2)$ can assume only discrete values, 0 or $-\pi$. Inset: the probability of observing the most probable trajectory with postselected readout sequence $\{r_k = +\}$ at $c = 2.1$; the grey dashed line indicates $P = 1$ for $c \to \infty$, showing the dynamical quantum Zeno effect.

one distinguishes three qualitatively different measurement regimes (cf. Fig. 3). In the limits of either strong or weak measurements, all trajectories except the one corresponding to $r_k = +$ for all k carry negligible probabilities. Therefore, the average GP approaches the value computed for the postselected trajectory in those limits. The absence of fluctuations in the GP and the near certainty of successful postselection in the final measurement implies that dephasing is absent ($\alpha \to 0$). Only in the intermediate regime, the distribution of trajectories is broadened; the average GP then noticeably deviates from the one in the postselected trajectory and dephasing emerges. Interestingly, the dephasing suppression factor accompanying the geometric phase follows the same behavior as the probability suppression of the postselected trajectory considered above. This indicates the fact that the postselected trajectory yields the dominant contribution, being often the most probable trajectory. Indeed, while the probability of this trajectory is $\mathcal{O}(1)$, all other trajectories contribute each with its own phase and a small weight.

Postselected geometric phase: topological nature of strong to weak measurement transition

We next study the dependence of the GP of the postselected trajectory with all outcomes $r_k = +$ on the measurement sequence polar angle θ for a given measurement strength. Consider the continuous function $\chi_{\rm geom}(\theta) : [0, \pi] \to \mathbb{R}$. (Note that although $\chi_{\rm geom}$ is a phase and is thus defined $\mod 2\pi$, we unfold it to have values in $\mathbb{R}$ by demanding that $\chi_{\rm geom}(0) = 0$ and that $\chi_{\rm geom}(\theta)$ is continuous). For $c \gg 1$ (i.e., $\eta_{\rm eff} \to 1$), it behaves as the standard Pancharatnam-Berry phase, $\chi_{\rm geom}(\theta) = \pi(\cos\theta - 1)$. For $c = 0$, $\chi_{\rm geom}(\theta) = 0$. We find that the regimes of infinitely weak and infinitely strong measurements are separated by a sharp transition, cf. Fig. 4. For $\theta = \pi/2$, the expression in the r.h.s. of Eq. (7) is real, implying that $\chi_{\rm geom}(\theta = \pi/2)$ can only take values 0 and $-\pi$. Thus, the interpolation of $\chi_{\rm geom}(\pi/2)$ between the infinitely

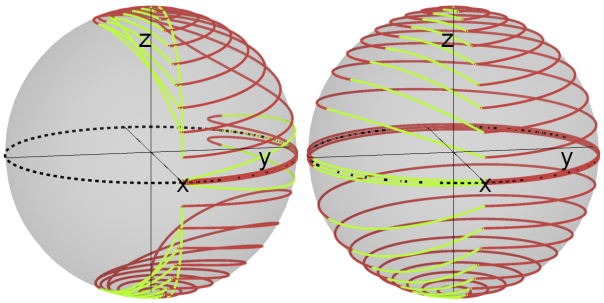

Fig. 5. Mapping of measurement sequences onto the system's quantum trajectories: a topological transition. A θ-dependent family of trajectories on the Bloch sphere for $c < c_{\rm crit}$ (left) and $c > c_{\rm crit}$ (right). Yellow segments represent final projective measurements, ascertaining closed trajectories. For stronger measurements (right), the S^2 space of the measurement orientations $\mathbf{n}$ is mapped through the measurement process onto the whole S^2 Bloch sphere of quantum trajectories. For weaker measurement strengths, the S^2 space of measurement orientations is mapped onto a subset of the Bloch sphere. The corresponding Chern numbers are -1 and 0, respectively.

weak and infinitely strong regimes must involve a discontinuous jump. As the measurement strength is reduced, we have $\chi_{\rm geom}(\pi/2) = -\pi$ to a critical strength, $c_{\rm crit} \approx 2.15$, below which $\chi_{\rm geom}(\pi/2) = 0$. Note also that $\chi_{\rm geom}(\theta)$ is a monotonic function for $c > c_{\rm crit}$ and is non-monotonic for $c < c_{\rm crit}$. At $c = c_{\rm crit}$, $\chi_{\rm geom}(\pi/2)$ is ill-defined as the probability of a successful postselection (i.e., that all readouts are $r_k = +$) $P(\theta = \pi/2) = 0$.

We relate these observations concerning the GP to the behavior of the induced quantum state trajectory at $\theta = \pi/2$, cf. Fig. 5. The quantum state trajectory for $\theta = \pi/2$ lies entirely on the equator of the Bloch sphere. For $c > c_{\rm crit}$, the trajectory after $N-1$ finite strength measurements $\left(\left|\psi_{\theta=\pi/2}(t \in [0,\pi])\right\rangle\right)$ traverses more than half the equator; the last projective measurement brings it back to the original point by the shortest geodesic, completing the circle around the equator. The solid angle subtended by the trajectory is then $\Omega = 2\pi$, and $\chi_{\rm geom}(\theta = \pi/2) = -\pi$. For $c < c_{\rm crit}$, $\left|\psi_{\pi/2}(\pi)\right\rangle$ has not reached the equator 's middle, and the last projective measurement again brings the system state back to the original point by the shortest geodesic, which in this case implies retracing its path back. The trajectory then subtends no solid angle, and the resulting phase $\chi_{\rm geom}(\theta = \pi/2) = 0$. Note that the existence of a sharp transition at $\theta = \pi/2$ is protected by the fact that $M_\eta(\mathbf{e}_z, r)$ is real, cf. Eq. (17), which guarantees that the trajectory always remains on the equator and thus $\chi_{\rm geom}(\pi/2) \in \{0, -\pi\}$.

This picture, in fact, extends beyond the trajectories on the equator. Consider the manifold formed by *all* state trajectories, which is obtained via measurement sequences at $\theta \in [0,\pi]$, cf. Fig. 5. For $c > c_{\rm crit}$, this manifold covers the Bloch sphere, while for subcritical c it does not. The GP transition then corresponds to a change in the topology of the set of state trajectories — thence the designation "topological transition". While this transition can be intuitively understood from the behavior of the trajectory on the equator, we prove it formally below (cf. Methods) by considering the Chern number

$$\mathcal{C} \equiv \frac{1}{2\pi}\int_0^{\pi} d\theta \int_0^{2\pi} dt\, \tilde{B}(\theta,t) = \frac{1}{2\pi}\left(\chi_{\rm geom}(\pi) - \chi_{\rm geom}(0)\right) \in \{0,-1\}, \quad [9]$$

where $\tilde{B}(\theta,t)$ is the Berry curvature

$$\tilde{B}(\theta,t) = \mathrm{Im}\left(\partial_t \langle\psi_\theta(t)|\, \partial_\theta\, |\psi_\theta(t)\rangle - \partial_\theta \langle\psi_\theta(t)|\, \partial_t\, |\psi_\theta(t)\rangle\right). \quad [10]$$

Transitions in quantum dynamics as a function of the measurement strength have been known for single qubits (29) and more recently discovered for many-body systems (31). Notably, the topological nature of the transition we report here is novel. Importantly, it implies that the transition is robust against perturbing the protocol. For example, if one considers sequences of measurements that follow generic closed curves different from the parallels considered above, it would not be possible to define $\chi_{\rm geom}(\pi/2)$ and determine the transition from its discrete set of values. However, as long as the family of measurement sequences wraps the sphere, there is a Chern number which assumes a discrete set of values (characterizing a global property of the set of measurement-induced trajectories) controlled by the measurement strength. Importantly, the Chern number is different in the limits of weak and strong measurements. This guarantees the existence of a critical measurement strength, $c_{\rm crit}$, at which the Chern number changes abruptly, and a concurrent jump of the phase $\chi_{\rm geom}$ associated with a critical measurement sequence. Unlike the transition, whose existence is protected by the change of the topological invariant, the value $c_{\rm crit}$ at which it takes place and the corresponding critical measurement sequence are non-universal and depend on the specifics of the protocol.

Experimental implementations

In order to detect the postselected GP in an experiment, we design a protocol based on a Mach-Zehnder interferometer incorporating detectors in one of its arms (cf. Fig. 6(a)). An impinging particle with an internal degree of freedom (spin for electrons, polarization for photons) in state $|\psi_0\rangle$ is split into two modes in the two interferometer arms. The compound system-detector state is then $|\Psi_i\rangle = |\psi_0\rangle \otimes (|a=1\rangle + |a=-1\rangle) \otimes |{+}...{+}\rangle/\sqrt{2}$, where $a = \pm 1$ describes the particle being in the upper or lower arm, respectively, and $|{+}...{+}\rangle$ is the initial state of the detectors. In the upper arm, the particle is subsequently measured by all the detectors; in addition it acquires an extra dynamical phase γ controlling the interference. Running through the lower arm, the state is left untouched. Traversing the interferometer, the state is then $|\Psi_f\rangle = |\psi_0\rangle\, |a=-1\rangle\, |{+}...{+}\rangle/\sqrt{2} + e^{i\gamma}\sum_{\{r_k\}}\prod_{k=1}^{N}\mathcal{M}_k^{(r_k)}|\psi_0\rangle\, |a=1\rangle\, |\{r_k\}\rangle/\sqrt{2}$, where r_k is the readout of the k-th measurement, and $|\{r_k\}\rangle$ is the corresponding collective state of all the detectors. The state with all readouts $r_k = +$ coincides with the initial state of all the detectors $|{+}...{+}\rangle$, therefore producing interference [*]. The

[*] Note that in this scheme we actually do not postselect the $\{r_k = +\}$ readout sequence but since only this sequence yields no "which-path" information, it is the only one giving rise to interference. Therefore, in the final interference, we only see the geometric phase of the $\{r_k = +\}$ trajectory.

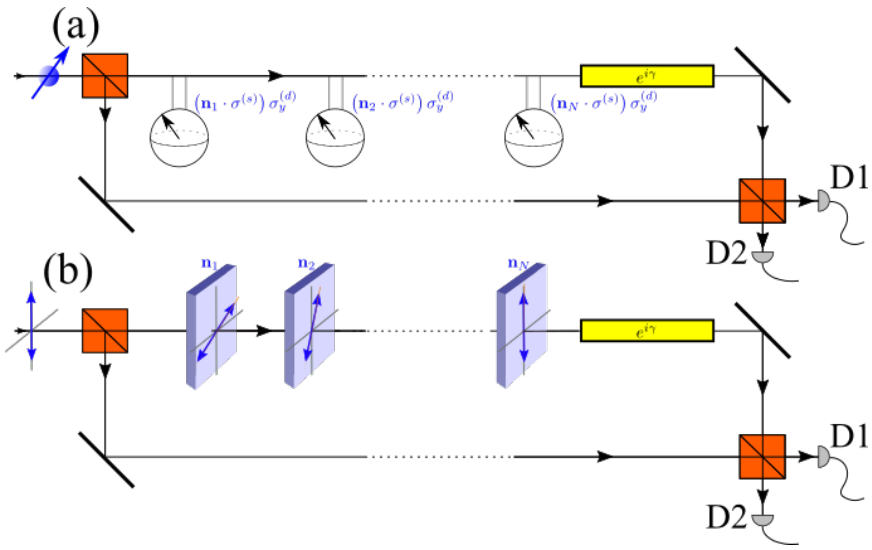

Fig. 6. Experimental setups for observing measurement-induced GPs. (a) Observing the postselected GP in a Mach-Zehnder interference setup. A particle interacts with a sequence of detectors in one arm. The null-type of the measurements employed means that the detectors do not change their state for $r_k = +$ readouts. No "which-path" information is implied, hence the GP acquired in the postselected readout sequence $\{r_k = +\}$ is manifest in the interference pattern at drains D1 and D2. (b) An equivalent setup with polarized photons as particles and imperfect polarizers acting as postselected weak measurements. In both setups, we assume an extra phase difference $e^{i\gamma}$ produced by means other than measurements.

intensities observed at drains D1 and D2 are

$$I_{1,2} = \frac{I_0}{2}\left(1 \pm \mathrm{Re}\, e^{i\gamma}\,\langle\psi_0|\prod_{k=1}^{N}\mathcal{M}_k^{(+)}|\psi_0\rangle\right) = \frac{I_0}{2}\left(1 \pm \sqrt{P}\mathrm{Re}\, e^{i\chi_{\mathrm{geom}}+i\gamma}\right), \quad [11]$$

where, for $N \to \infty$, $\sqrt{P}e^{i\chi_{\mathrm{geom}}}$ is given by Eq. (7) and I_0 is the intensity of the incoming particle beam. The probability of a successful postselection $P = P_{\{r_k=+\}}$ thus determines the interference visibility, and the weak-measurement-induced phase χ_{geom} is directly related to the interference phase. Note that the null-type measurements are essential here as they induce backaction without forming a "which-path" signature, thus facilitating interference.

In practice, this protocol can be implemented employing imperfect optical polarizers (cf. Fig. 6(b)). An imperfect polarizer can transmit (readout $+$) or absorb (readout $-$) the impinging light. More specifically, each polarizer fully transmits one given polarization ($|+\mathbf{n}_k\rangle$) and partially absorbs the orthogonal one ($|-\mathbf{n}_k\rangle$). A transmitted beam corresponds to a $+$ readout, thus implementing a postselected null-type measurement considered above (cf. Eq. (4)). By rotating the polarizers and adding phase plates (e.g., quarter-wave plates), it is possible to control the orientation $|+\mathbf{n}_k\rangle$ that is fully transmitted. The larger the probability to absorb a photon of polarization $|-\boldsymbol{n}_k\rangle$, the stronger the measurement is. The polarization state of a beam traversing the sequence of polarizers reproduces the postselected state with all readouts $r_k = +$. Installing a set of polarizers in one of the interferometer's arms would allow us to detect the postselected GP through the interference pattern. The obtained signals at the interferometer outputs D1 and D2 are

$$I_{1,2} = I_0\left(\frac{1+P}{4} \pm \frac{1}{2}\sqrt{P}\mathrm{Re}\, e^{i\chi_{\mathrm{geom}}+i\gamma}\right) = \frac{I_0}{4}\left|1 \pm \sqrt{P}e^{i\chi_{\mathrm{geom}}+i\gamma}\right|^2. \quad [12]$$

The GP can be extracted from the interference pattern controlled by γ. The difference in the intensities compared to Eq. (11) accounts for the loss due to the light absorption by the imperfect polarizers. Note that the limit of polarizers corresponding to strong measurements (i.e., one polarization of the beam is fully transmitted while the orthogonal polarization is fully blocked) is a realization of the Pancharatnam phase ((15, 18)). The polarizers must be carefully designed such that no additional phase difference between the two polarizations is accumulated by the light passing through a polarizer. This is particularly important because the topological nature of the transition investigated above is protected by the hermiticity of the Kraus operators, $\mathcal{M}_k^{(r_k)}$. [†]

The above protocol can also be implemented using superconducting qubit hardware (23–26). In such an implementation, the particle's internal degree of freedom is replaced by the two lowest levels of a superconducting Josephson junction (which form the qubit). The lower reference arm of the interferometer should be then replaced by an extra level that is unaffected by the measurements.

Discussion

We have shown how sequences of generalized quantum measurements may modify the phase of the state of the system measured, inducing a purely geometric phase. In other words, the trajectory traced by the quantum state can be directly mapped onto the phase accrued during the sequence of measurements. As opposed to geometric phases induced by an adiabatic Hamiltonian evolution, the phases obtained here depend on the measurement strength and are inherently stochastic. We have put forward schematic experimental protocols for measuring the geometric phase associated with a specific postselected readout sequence (in other words: of a specific postselected trajectory). We have shown that the mapping of measurement sequences to geometric phases undergoes a topological transition as the measurement strength is varied. This transition is classified through a jump of a Chern number. This transition is also manifest through an abrupt change of the dependence of the geometric phase on the polar angle, θ, of the measurement sequence from a monotonous to a non-monotonous one. An analysis of the averaged geometric phases in the Supplementary material shows a similar feature

[†] An investigation of the weak-measurement-induced geometric phase when the Kraus operators are non-Hermitian will be performed elsewhere.

in the θ-dependence. Our analysis underscores for the first time the topological nature of a strong-to-weak measurement transition.

The transition prevails in a much broader context, which is guaranteed by its topological nature. Since the Chern numbers in the limit of strong measurements and in the limit of infinitely weak measurements are different, the transition will take place also for measurements of different types, characterized by Kraus operators other than the ones we used (yet still Hermitian). Further, while we investigated quasicontinuous ($N \to \infty$) sequences of weak measurements, the transition will take place for any number $N \geq 3$ of measurements (albeit the critical measurement strength will depend on N).

We believe that the interplay between the topological nature of the measurement and possible topological structure of the system measured (associated with, e.g., non-Abelian quasiparticles, band structure and dynamical evolution) opens an intriguing horizon.

Materials and Methods

Measurement model. The measurement sequence leading to the geometric phase in Eq. (3) consists of positive-operator valued measurements (POVMs) defined by the Kraus operators $\mathcal{M}_k^{(r_k)} = M_{\eta_k}(\mathbf{n}_k, r_k)$, $|\psi\rangle \to \mathcal{M}_k^{(r_k)}|\psi\rangle$, as described in the main text. Such POVMs can be implemented with a detection apparatus consisting of a second qubit, whose Hilbert space is spanned by $|+\rangle$ and $|-\rangle$ and which is coupled to the system via the Hamiltonian

$$H_{\mathbf{n}}(t) = \lambda(t)(1-\sigma_{\mathbf{n}}^{(s)})\sigma_y^{(d)}/2. \quad [13]$$

Here, $\sigma^{(s/d)}$ denote the Pauli matrices acting on the system and detector, respectively, $\sigma_{\mathbf{n}} = \mathbf{n}\cdot\boldsymbol{\sigma}$ and $\mathbf{n} = (\sin\theta\cos\varphi, \sin\theta\sin\varphi, \cos\theta)$, $0 \leqslant \theta \leqslant \pi$, $0 \leqslant \varphi < 2\pi$, defines the measurement direction. The system and detector are initially ($t = 0$) decoupled in the state $|\psi_s^{(\mathrm{in})}\rangle \otimes |+\rangle$, where

$$|\psi_s^{(\mathrm{in})}\rangle = a\,|\uparrow\rangle + b\,|\downarrow\rangle = \begin{pmatrix} a \\ b \end{pmatrix}. \quad [14]$$

The measurement coupling $\lambda(t) \neq 0$ is then switched on for $t \in [0, T]$ to obtain the entangled state:

$$\begin{aligned} |\psi_{\mathrm{ent}}\rangle &= \exp\left[-ig(1-\sigma_{\mathbf{n}}^{(s)})\sigma_y^{(d)}/2\right]|\psi_s^{(\mathrm{in})}\rangle\,|+\rangle \\ &= M_\eta(\mathbf{n},+)|\psi_s^{(\mathrm{in})}\rangle\,|+\rangle + M_\eta(\mathbf{n},-)|\psi_s^{(\mathrm{in})}\rangle\,|-\rangle\,. \end{aligned} \quad [15]$$

Here, $g = \int_0^T dt\lambda(t)$ determines the measurement strength $\eta = \sin^2 g$. The matrices $M_\eta(\mathbf{n},+)$ and $M_\eta(\mathbf{n},-)$ are defined by

$$M_\eta(\mathbf{n}, r) = R^{-1}(\mathbf{n})M_\eta(\mathbf{e}_z, r)R(\mathbf{n}), \quad [16]$$

where

$$M_\eta(\mathbf{e}_z,+) = \begin{pmatrix} 1 & 0 \\ 0 & \sqrt{1-\eta} \end{pmatrix},\ M_\eta(\mathbf{e}_z,-) = \begin{pmatrix} 0 & 0 \\ 0 & \sqrt{\eta} \end{pmatrix} \quad [17]$$

are the Kraus operators for the measurement orientation along the z axis ($\mathbf{n} = \mathbf{e}_z$) and

$$R(\mathbf{n}) = \begin{pmatrix} \cos\theta/2 & e^{-i\varphi}\sin\theta/2 \\ \sin\theta/2 & -e^{-i\varphi}\cos\theta/2 \end{pmatrix} \quad [18]$$

is a unitary matrix corresponding to the rotation of the measurement orientation $|\pm\mathbf{n}\rangle = R^{-1}(\mathbf{n})|\pm\mathbf{e}_z\rangle = R^{-1}(\mathbf{n})|\uparrow/\downarrow\rangle$. This implements a null-type weak measurement as defined in the main text.

Geometric phase from a quasicontinuous measurement sequence and postselection. The geometric phase χ_{geom} obtained from the quasicontinuous trajectory with all outcomes $r_k = +$ is given in Eq. (7). This result is obtained starting from Eq. (3). By setting $|\psi_0\rangle = R^{-1}(\mathbf{n}_0)\,|\uparrow\rangle$, the readouts $r_k = +$ and the measurement orientations $(\theta_k, \varphi_k) = (\theta, 2\pi k/N)$, and using the explicit form of Kraus operators in Eq. (16), one rewrites

$$\langle\psi_0|\,\mathcal{M}_{N-1}^{(+)}\ldots\mathcal{M}_1^{(+)}\,|\psi_0\rangle = \langle\uparrow|\,\delta R\left(M_{\eta=4c/N}(\mathbf{e}_z,+)\delta R\right)^{N-1}|\uparrow\rangle\,, \quad [19]$$

where

$$\begin{aligned} \delta R &= R(\mathbf{n}_{k+1})R^{-1}(\mathbf{n}_k) \\ &= \begin{pmatrix} \cos^2\frac{\theta}{2} + e^{-2\pi i/N}\sin^2\frac{\theta}{2} & \frac{1}{2}(1-e^{-2\pi i/N})\sin\theta \\ \frac{1}{2}(1-e^{-2\pi i/N})\sin\theta & \sin^2\frac{\theta}{2} + e^{-2\pi i/N}\cos^2\frac{\theta}{2} \end{pmatrix} \end{aligned} \quad [20]$$

is a matrix independent of k. The quasicontinuous limit is obtained by diagonalizing the 2×2 matrix $M_{\eta=4c/N}(\mathbf{e}_z,+)\delta R$ and calculating the matrix elements in Eq. (19) in the limit $N \to \infty$. This yields Eq. (7).

Chern number for the mapping of measurement orientations onto state trajectories. The mapping of quasicontinuous measurements orientations onto state trajectories is topologically classified by the Chern number in Eq. (9). The discrete values of the Chern number are in correspondence with the different regimes of the θ-dependence of $\chi_{\mathrm{geom}}(\theta)$. To prove this, we parametrize each state $|\psi_\theta(t)\rangle$, $\theta \in [0,\pi]$, $t \in [0, 2\pi]$, as $|\psi_\theta(t)\rangle = e^{i\alpha(\theta,t)}(\cos\frac{\Theta(\theta,t)}{2}\,|\uparrow\rangle + \sin\frac{\Theta(\theta,t)}{2}e^{i\Phi(\theta,t)}\,|\downarrow\rangle) = e^{i\alpha(\theta,t)}\,|\Psi(\Theta,\Phi)\rangle$ with (Θ,Φ) being coordinates on the Bloch sphere. Since $|\psi_\theta(2\pi)\rangle = |\psi_\theta(0)\rangle$ and $\left|\psi_{\theta=0,\pi}(t)\right\rangle = \left|\psi_{\theta=0,\pi}(0)\right\rangle$, the parameters t and θ can be regarded as a parametrization of a sphere, and the map $(\theta,t) \mapsto (\Theta,\Phi)$ is equivalent to the mapping of a sphere to a sphere $\mathcal{F}: S^2 \ni (\theta,t) \mapsto (\Theta,\Phi) \in S^2$.

In the quasicontinuous limit, the Pancharatnam phase in Eq. (1) reduces to the Berry phase accumulated by $|\Psi\rangle$ and can be computed by standard methods (3) to express it as an integral of the Berry curvature. In fact, for any $\theta_0 \in [0,\pi]$, we have $\chi_{\mathrm{geom}}(\theta_0) = \int_0^{\theta_0}\int_0^{2\pi} d\theta dt\,\tilde{B}(\theta,t)$ (see Eq. (21)).

where $\tilde{B}(\theta,t)$ is the Berry curvature introduced in Eq. (10). Alternatively, using the mapping $\mathcal{F}: (\theta,t) \mapsto (\Theta,\Phi)$, the geometric phase can be expressed in terms of a curvature on the Bloch sphere as

$$\begin{aligned} \chi_{\mathrm{geom}}(\theta_0) - \chi_{\mathrm{geom}}(0) &= \int_0^{\theta_0}\int_0^{2\pi} d\theta dt\,\tilde{B}(\theta,t) \\ &= \int_0^{\theta_0}\int_0^{2\pi} d\theta dt\,\frac{\partial(\Theta,\Phi)}{\partial(\theta,t)}B(\Theta,\Phi), \end{aligned} \quad [22]$$

with

$$\begin{aligned} B(\Theta,\Phi) &= \frac{\partial(\theta,t)}{\partial(\Theta,\Phi)}\tilde{B}(\theta(\Theta,\Phi),t(\Theta,\phi)) \\ &= -\,\mathrm{Im}\left(\partial_\Theta\langle\Psi(\Theta,\Phi)|\,\partial_\Phi|\Psi(\Theta,\Phi)\rangle\right. \\ &\qquad \left. -\,\partial_\Phi\langle\Psi(\Theta,\Phi)|\,\partial_\Theta|\Psi(\Theta,\Phi)\rangle\right) \\ &= -\frac{1}{2}\sin\Theta(\theta,t), \end{aligned} \quad [23]$$

and where

$$\frac{\partial(\Theta,\Phi)}{\partial(\theta,t)} = \frac{\partial\Theta}{\partial\theta}\frac{\partial\Phi}{\partial t} - \frac{\partial\Theta}{\partial t}\frac{\partial\Phi}{\partial\theta} \quad [24]$$

is the Jacobian of $\mathcal{F}$.

The r.h.s. of Eq. (22) admits a simple interpretation: $\chi_{\mathrm{geom}}(\theta_0) - \chi_{\mathrm{geom}}(0) = -\mathcal{A}_{\theta_0}/2$, where $\mathcal{A}_{\theta_0}$ is the oriented area of the Bloch sphere covered by the measurement-induced trajectories $|\Psi(\Theta(\theta,t),\Phi(\theta,t))\rangle$ with $\theta \in [0,\theta_0]$ (here the orientation of each infinitesimal contribution is given by the sign of the Jacobian). In particular, for $\theta_0 = \pi$, $\mathcal{A}_\pi = 4\pi$ if the surface generated by all the trajectories wraps the Bloch sphere once, and $\mathcal{A}_\pi = 0$ if it does not wrap around the Bloch sphere, cf. Fig. 5. This provides the two

$$\chi_{\rm geom}(\theta_0) = \chi_{\rm geom}(\theta_0) - \chi_{\rm geom}(0) = \arg \prod_{t=0}^{2\pi - dt} \langle \Psi(\Theta(\theta_0, t+dt), \Phi(\theta_0, t+dt)) | \Psi(\Theta(\theta_0, t), \Phi(\theta_0, t)) \rangle$$
$$= i \int_0^{2\pi} dt \, \langle \Psi(\Theta(\theta_0, t), \Phi(\theta_0, t)) | \, \partial_t \, | \Psi(\Theta(\theta_0, t), \Phi(\theta_0, t)) \rangle$$
$$= -\mathrm{Im} \int_0^{\theta_0} \int_0^{2\pi} d\theta dt \, (\partial_\theta \langle \Psi(\Theta, \Phi) | \, \partial_t \, | \Psi(\Theta, \Phi) \rangle - \partial_t \langle \Psi(\Theta, \Phi) | \, \partial_\theta \, | \Psi(\Theta, \Phi) \rangle)$$
$$= \int_0^{\theta_0} \int_0^{2\pi} d\theta dt \, \tilde{B}(\theta, t), \qquad [21]$$

possible values for the Chern number (9) $\mathcal{C} \in \{0, -1\}$. Formally, this can be proven by explicitly using the degree of the map $\mathcal{F}$ (32). The degree of the map $\mathcal{F}$, $\deg \mathcal{F}$, is the number of points (θ, t) that map to a given point (Θ, Φ) (provided that (Θ, Φ) is a regular point of $\mathcal{F}$) taking the orientation into account. The degree does not depend on the specific point (Θ, Φ) and can be expressed as

$$\deg \mathcal{F} = \sum_{(\theta,t) \in \mathcal{F}^{-1}[(\Theta,\Phi)]} \mathrm{sgn} \frac{\partial(\Theta, \Phi)}{\partial(\theta, t)}, \qquad [25]$$

where $\mathcal{F}^{-1}[(\Theta, \Phi)]$ is the set of points (θ, t) that are mapped by $\mathcal{F}$ into (Θ, Φ), and sgn is the sign function. Considering the integral as the sum of infinitesimal contributions and grouping those by the image points (Θ, Φ), one then shows that

$$\int_0^{\pi} \int_0^{2\pi} d\theta dt \, \frac{\partial(\Theta, \Phi)}{\partial(\theta, t)} \sin \Theta(\theta, t) = 4\pi \deg \mathcal{F}. \qquad [26]$$

This topological feature is reflected in the discrete value of $\chi_{\rm geom}(\pi/2)$, hence in the θ-dependence of $\chi_{\rm geom}$. To show this, note that Eq. (7) is symmetric under complex conjugation supplemented by $\theta \to \pi - \theta$, i.e. $\chi_{\rm geom}(\pi - \theta) = -\chi_{\rm geom}(\theta) \mod 2\pi$. Using the continuity of $\chi_{\rm geom}(\theta)$, we obtain $\chi_{\rm geom}(\pi - \theta) = -\chi_{\rm geom}(\theta) + 2\chi_{\rm geom}(\pi/2)$, and hence (for $\theta = 0$), $\chi_{\rm geom}(\pi/2) = (\chi_{\rm geom}(\pi) + \chi_{\rm geom}(0))/2 = \chi_{\rm geom}(\pi)/2 = \pi\mathcal{C}$. Therefore, we have $\chi_{\rm geom}(\pi/2) = \pi\mathcal{C} = -\pi$ for $c > c_{\rm crit}$ and $\chi_{\rm geom}(\pi/2) = \pi\mathcal{C} = 0$ for $c < c_{\rm crit}$ as shown in Fig. 4.

Monte Carlo numerical simulations. The results for the averaged GP have been obtained using a Monte Carlo simulation of the sum over different measurement readouts $\{r_k\}_{k=1,\ldots,N-1}$. We simulated the sequences of measurement readouts taking their probabilities $P_{\{r_k, r_N=+\}} = \left|\langle\psi_0|\tilde{\psi}_{N-1}\rangle\right|^2 = \left|\langle\psi_0| \, \mathcal{M}_{N-1}^{(r_{N-1})} \ldots \mathcal{M}_1^{(r_1)} \, |\psi_0\rangle\right|^2 = |\langle\psi_0| \, M_\eta(\mathbf{n}_{N-1}, r_{N-1}) \ldots M_\eta(\mathbf{n}_1, r_1) \, |\psi_0\rangle|^2$ into account. Namely, the quasicontinuous trajectory was represented by $N = 500$ measurements ($N - 1 = 499$ weak measurements and one strong postselected measurement). For the k-th measurement, we calculated $|\psi_k'(r_k)\rangle = M_\eta(\mathbf{n}_k, r_k) \, |\psi_{k-1}\rangle \propto \left|\tilde{\psi}_k\right\rangle$ ($|\psi_k\rangle$ is the normalization of $\left|\tilde{\psi}_k\right\rangle$, which in turn has been defined in Eq. (2)) and randomly determined the measurement readout $r_k = +/-$ according to probabilities $p(r_k) = \langle\psi_k'(r_k)|\psi_k'(r_k)\rangle$. Then, for the selected r_k, the normalized state $|\psi_k\rangle = \left|\psi_k'(r_k)\right\rangle / \sqrt{p(r_k)}$ was calculated; after which the next measurement was simulated. After simulating $N-1$ weak measurements, $z_{\{r_k\}} = z(\text{realization}) = (\langle\psi_0|\psi_{N-1}\rangle)^2 = P_{\{r_N=+\}} e^{2i\chi_{\rm geom}(\{r_k\})}$ was determined. After repeating this simulation $N_{\rm realizations}$ times, $e^{i2\bar{\chi}_{\rm geom} - \alpha} = \langle e^{2i\chi_{\rm geom}}\rangle_{\rm realizations} = N_{\rm realizations}^{-1} \sum_{\rm realizations} z(\text{realization})$ was calculated. Fig. 3 was obtained using $N_{\rm realizations} = 4000$.

Data availability. All the data regarding the postselected geometric phase have been produced by means of an analytical formula, Eq. (7). The distribution of the geometric phases in the absence of postselection and the averaged geometric phase (Fig. 3) have been plotted based on the data produced by Monte Carlo simulations according to the algorithm described above. The code implementing the simulations and the relevant data can be found at https://github.com/KyryloSnizhko/top-geom-meas.

ACKNOWLEDGMENTS. V.G. thanks T. Holder for helpful discussions. V.G. acknowledges financial support by the Minerva foundation under the Short-Term Research Grant programme. K.S. and Y.G. acknowledge funding by the Deutsche Forschungsgemeinschaft (DFG, German Research Foundation) – Projektnummer 277101999 – TRR 183 (project C01). A.R. acknowledges support from EPSRC via Grant No. EP/P010180/1.

1. M. Born and V. Fock. Beweis des Adiabatensatzes. *Zeitschrift für Phys.*, 51(3-4):165–180, 1928. ISSN 14346001. . URL https://link.springer.com/content/pdf/10.1007{%}2FBF01343193.pdf.
2. A Messiah. *Quantum Mechanics*. Dover Publications, 1961.
3. M. V. Berry. Quantal Phase Factors Accompanying Adiabatic Changes. *Proc. R. Soc. A Math. Phys. Eng. Sci.*, 392(1802):45–57, 1984. ISSN 1364-5021. . URL http://rspa.royalsocietypublishing.org/cgi/doi/10.1098/rspa.1984.0023.
4. Frank Wilczek and Alfred Shapere. *Geometric phases in physics*. World Scientific, 1989.
5. Di Xiao, Ming Che Chang, and Qian Niu. Berry phase effects on electronic properties. *Rev. Mod. Phys.*, 82(3):1959–2007, 2010. ISSN 00346861. . URL https://journals.aps.org/rmp/pdf/10.1103/RevModPhys.82.1959.
6. Dariusz Chruscinski and Andrzej Jamiolkowsk. *Geometric Phases in Classical and Quantum Mechanics*. Springer Science & Business Media, New York, 2012.
7. D J Thouless, M Kohmoto, M P Nightingale, and M den Nijs. Quantized Hall Conductance in a Two-Dimensional Periodic Potential. *Phys. Rev. Lett.*, 49(6):405–408, aug 1982. ISSN 0031-9007. . URL https://journals.aps.org/prl/pdf/10.1103/PhysRevLett.49.405https://link.aps.org/doi/10.1103/PhysRevLett.49.405.
8. B. A. Bernevig. *Topological Insulators and Topological Superconductors*. Princeton University Press, 2013.
9. János K. Asbóth, László Oroszlány, and András Pályi. *A short course on topological insulators*. Springer International Publishing, 2016.
10. Frank Wilczek. *Fractional Statistics and Anyon Superconductivity*. World Scientific Publishing, Singapore, 1990.
11. K. T. Law, D. E. Feldman, and Yuval Gefen. Electronic Mach-Zehnder interferometer as a tool to probe fractional statistics. *Phys. Rev. B*, 74(4):045319, jul 2006. ISSN 1098-0121. . URL https://link.aps.org/doi/10.1103/PhysRevB.74.045319.
12. Shi-Liang Zhu and Paolo Zanardi. Geometric quantum gates that are robust against stochastic control errors. *Phys. Rev. A*, 72(2):020301, aug 2005. ISSN 1050-2947. . URL https://link.aps.org/doi/10.1103/PhysRevA.72.020301.
13. Chetan Nayak, Steven H. Simon, Ady Stern, Michael Freedman, and Sankar Das Sarma. Non-Abelian anyons and topological quantum computation. *Rev. Mod. Phys.*, 80(3):1083–1159, sep 2008. ISSN 0034-6861. . URL https://link.aps.org/doi/10.1103/RevModPhys.80.1083.
14. Y. Aharonov and J. Anandan. Phase change during a cyclic quantum evolution. *Phys. Rev. Lett.*, 58(16):1593–1596, apr 1987. ISSN 0031-9007. . URL https://link.aps.org/doi/10.1103/PhysRevLett.58.1593.
15. S. Pancharatnam. Generalized theory of interference, and its applications. *Proc. Indian Acad. Sci. - Sect. A*, 44(5):247–262, nov 1956. ISSN 0370-0089. . URL http://link.springer.com/10.1007/BF03046050.
16. Joseph Samuel and Rajendra Bhandari. General Setting for Berry's Phase. *Phys. Rev. Lett.*, 60(23):2339–2342, jun 1988. ISSN 0031-9007. . URL https://link.aps.org/doi/10.1103/PhysRevLett.60.2339.
17. P. Facchi, A.G. Klein, S. Pascazio, and L.S. Schulman. Berry phase from a quantum Zeno effect. *Phys. Lett. A*, 257(5-6):232–240, jul 1999. ISSN 03759601. . URL https://linkinghub.elsevier.com/retrieve/pii/S0375960199003230.
18. M. V. Berry and S. Klein. Geometric phases from stacks of crystal plates. *J. Mod. Opt.*, 43(1):165–180, jan 1996. ISSN 0950-0340. . URL http://www.tandfonline.com/doi/abs/10.1080/09500349608232731.
19. Yakir Aharonov, David Z. Albert, and Lev Vaidman. How the result of a measurement of a component of the spin of a spin- 1/2 particle can turn out to be 100. *Phys. Rev. Lett.*, 60(14):

1351–1354, apr 1988. ISSN 0031-9007. . URL https://link.aps.org/doi/10.1103/PhysRevLett.60.1351.
20. Young-Wook Cho, Yosep Kim, Yeon-Ho Choi, Yong-Su Kim, Sang-Wook Han, Sang-Yun Lee, Sung Moon, and Yoon-Ho Kim. Emergence of the geometric phase from quantum measurement back-action. *Nat. Phys.*, apr 2019. ISSN 1745-2473. . URL http://www.nature.com/articles/s41567-019-0482-z.
21. K. Jacobs. *Quantum Measurement Theory and its Applications*. Cambridge University Press, Cambridge, 2014.
22. H. M. Wiseman and G. J. Milburn. *Quantum Measurement and Control*. Cambridge Univerity PRess, Cambridge, 2010.
23. K. W. Murch, S. J. Weber, C. Macklin, and I. Siddiqi. Observing single quantum trajectories of a superconducting quantum bit. *Nature*, 502(7470):211–214, oct 2013. ISSN 0028-0836. . URL http://www.nature.com/articles/nature12539.
24. S. J. Weber, A. Chantasri, J. Dressel, A. N. Jordan, K. W. Murch, and I. Siddiqi. Mapping the optimal route between two quantum states. *Nature*, 511(7511):570–573, jul 2014. ISSN 0028-0836. . URL http://www.nature.com/articles/nature13559.
25. M Naghiloo, D Tan, P M Harrington, J J Alonso, E Lutz, A Romito, and K W Murch. Heat and work along individual trajectories of a quantum bit. Technical report, 2019. URL https://arxiv.org/pdf/1703.05885.pdf.
26. Z. K. Minev, S. O. Mundhada, S. Shankar, P. Reinhold, R. Gutiérrez-Jáuregui, R. J. Schoelkopf, M. Mirrahimi, H. J. Carmichael, and M. H. Devoret. To catch and reverse a quantum jump mid-flight. *Nature*, 570(7760):200, jun 2019. ISSN 0028-0836. . URL http://www.nature.com/articles/s41586-019-1287-z.
27. Oded Zilberberg, Alessandro Romito, David J. Starling, Gregory A. Howland, Curtis J. Broadbent, John C. Howell, and Yuval Gefen. Null Values and Quantum State Discrimination. *Phys. Rev. Lett.*, 110(17):170405, apr 2013. ISSN 0031-9007. . URL https://link.aps.org/doi/10.1103/PhysRevLett.110.170405.
28. Oded Zilberberg, Alessandro Romito, and Yuval Gefen. Standard and Null Weak Values. In *Quantum Theory A Two-Time Success Story*, pages 377–387. Springer Milan, Milano, 2014. . URL http://link.springer.com/10.1007/978-88-470-5217-8{_}25.
29. Rusko Ruskov, Ari Mizel, and Alexander N. Korotkov. Crossover of phase qubit dynamics in the presence of a negative-result weak measurement. *Phys. Rev. B*, 75(22):220501, jun 2007. ISSN 1098-0121. . URL https://link.aps.org/doi/10.1103/PhysRevB.75.220501.
30. Pier A. Mello. The von Neumann model of measurement in quantum mechanics. pages 136–165, 2014. . URL http://aip.scitation.org/doi/abs/10.1063/1.4861702.
31. M. Szyniszewski, A. Romito, and H. Schomerus. Entanglement transition from variable-strength weak measurements. *Phys. Rev. B*, 100:064204, Aug 2019. . URL https://link.aps.org/doi/10.1103/PhysRevB.100.064204.
32. L. Ambrosio and N. Dancer. *Calculus of Variations and Partial Differential Equations*. Springer, Berlin Heidelberg, 2000.

Supplementary material

In this supplementary material, we focus on the full distribution of trajectories and we define and study the averaged geometric phase (GP). Subsequently, we propose an experimental protocol for the detection of such an averaged phase based on Mach-Zehnder interferometry. Throughout this Supplementary material, we use the same notation introduced in the manuscript.

1. Averaged geometric phase and its topological transition

The most sensible way to define the averaged geometric phase for the full distribution of trajectories is by appealing to averaging physically measurable observables. Below, we propose a possible experimental setup for detecting the GP, which introduces a direct protocol for averaging over numerous closed trajectories. The averaged geometric phase $\bar{\chi}_{\rm geom}$ is then defined through

$$e^{2i\bar{\chi}_{\rm geom}-\alpha} := \langle e^{2i\chi_{\rm geom}}\rangle_{\rm realizations} = \sum_{\{r_k\}} \left(\langle\psi_0| \mathcal{M}_{N-1}^{(r_{N-1})} \dots \mathcal{M}_1^{(r_1)} |\psi_0\rangle \right)^2 , \qquad [27]$$

where $\chi_{\rm geom}$ is the geometric phase associated with each single trajectory as introduced in the paper, $e^{-\alpha}$ is a suppression factor representing the suppression of the visibility of interference in the experimental setup (cf. Section 2 below) and the sum extends over all possible measurement readouts $\{r_k\}$. The suppression factor accounts for two effects: (i) the probability of a successful postselection in the final strong measurement that ensures that the state trajectory is closed, and (ii) "dephasing" due to $\chi_{\rm geom}$ having a spread of values for different trajectories. The behavior of the averaged GP $\bar{\chi}_{\rm geom}$ as a function of the measurement strength has been reported in the paper (cf. Fig. (3) therein).

The dependence of the averaged GP $\bar{\chi}_{\rm geom}(\theta)$ on the polar angle θ of the measurement sequence presents a transition as a function of the measurement strength in analogy to the case of postselected measurement sequences (cf. Fig. 7). Yet, the features of the transition are different. We begin by noting that $\bar{\chi}_{\rm geom}$ is defined only $\mod \pi$ (cf. Eq. (27)) , i.e., $\bar{\chi}_{\rm geom}$ is defined on a circle S^1 of circumference π. This makes a difference for the possible values of $\bar{\chi}_{\rm geom}$ at $\theta = \pi/2$: We have $\bar{\chi}_{\rm geom}(0) = 0$ as in the postelected case but at the equator $\theta = \pi/2$, where the possible values of $\chi_{\rm geom}$ are only 0 and $-\pi$, both values correspond to $e^{2i\chi_{\rm geom}} = 1$ implying $\bar{\chi}_{\rm geom}(\theta = \pi/2) = 0$. Hence, $\bar{\chi}_{\rm geom}(\theta)$ obeys periodic boundary conditions $\bar{\chi}_{\rm geom}(\pi/2) = \bar{\chi}_{\rm geom}(0)$, allowing us to identify the points $\theta = 0$ and $\theta = \pi/2$ such that θ can be defined on a circle S^1 of circumference $\pi/2$. Therefore, $\bar{\chi}_{\rm geom} : S^1 \ni \theta \mapsto \bar{\chi}_{\rm geom} \in S^1$ maps a circle onto a circle and can be classified by an integer-valued winding number m (how many times the function $\bar{\chi}_{\rm geom}(\theta)$ winds around the circle S^1 of length π as θ varies from 0 to $\pi/2$). In the limit of infinitely weak measurements, we have $\bar{\chi}_{\rm geom}(\theta) \equiv 0$, yielding $m = 0$. In the limit of strong projective measurements, however, $\bar{\chi}_{\rm geom}(\theta) = \pi(\cos\theta - 1)$, yielding $m = -1$. If the function $\chi_{\rm geom}(\theta)$ would depend continuously on the measurement strength, m would be preserved by increasing the measurement strength, which is incompatible with the two limiting cases of strong and infinitely weak measurements. Therefore, one expects a sharp transition at an intermediate measurement strength $c = \bar{c}_{\rm crit}$, marking the jump between these two different behaviors of $\bar{\chi}_{\rm geom}(\theta)$. At this critical measurement strength, $\bar{\chi}_{\rm geom}(\theta)$ is ill-defined for a certain polar angle $\bar{\theta}_{\rm crit}$. At these critical parameters ($\bar{\theta}_{\rm crit} \approx \pi/3$ with $c_{\rm crit} \approx 3.35$), the visibility $e^{-\alpha}$ vanishes, cf. Fig. 7 (inset).

With the $\{r_k = +\}$ readout sequence being the most probable, one naively expects the transition to take place near $c_{\rm crit} \approx 2.15$. However, precisely at the postselected transition ($c_{\rm crit} \approx 2.15$, $\theta_{\rm crit} = \pi/2$), the probability of this readout sequence vanishes, rendering phase averaging over the remaining trajectories a crucial factor. The actual transition happens at $\bar{c}_{\rm crit} \approx 3.35$ and $\bar{\theta}_{\rm crit} \approx \pi/3$, when the contribution of the $\{r_k = +\}$ readout sequence is cancelled against the phase-averaged contribution of the remaining sequences.

2. Detection of the averaged geometric phase via Mach-Zehnder interferometry

In order to observe the averaged measurement induced GP, we propose an interferometric setup along the lines of the detection scheme described for the detection of the postselected GP in the manuscript. Here, however, a different approach to coupling the detectors to the polarization of the beam in the interferometer arms is needed. Indeed, we need to account for all readout sequences $\{r_k\}$. Given the initial detector state $+$, a readout $r_k = -$ may serve as a "which-path" detection, undermining the interference (the readout $r_k = +$ used for the postselected trajectory in the manuscript does not provide "which-path" information due to the properties of the null-type measurement we use). The only way to overcome this handicap is to couple each detector to the two interferometer arms, making it impossible to deduce from the readout signal which arm the particle went through. This is demonstrated in Fig. 8. The $k-$th detector couples to $\sigma_{\mathbf{n}_k} = \boldsymbol{\sigma}\cdot\mathbf{n}_k$ in the upper arm and to $\sigma_{-\mathbf{n}_k} = -\sigma_{\mathbf{n}_k}$ in the lower arm of the interferometer. In addition, the particle's inner degree of freedom in the lower arm is flipped before and flipped back after the sequence of measurements. As a result, for any given readout sequence $\{r_k\}$, the trajectory on the Bloch sphere corresponding to the lower arm is exactly opposite to that of the upper arm (i.e., it is inverted with respect to the origin). It follows that the solid angle Ω subtended by the trajectories and the geometric phase $\chi_{\rm geom}$ accumulated through the upper and the lower arms have opposite signs but same magnitudes. Moreover, the probabilities $P_{\{r_k\}}$ for yielding the specific readout sequence $\{r_k\}$ are exactly the same in the two arms. This measurement scheme is thus completely devoid of "which-path" signals. Provided that the N-th measurement is postselected to yield $r_N = +$ and the runs with $r_N = -$ do not contribute to the readings at drains D1 and D2, the resulting intensities are

$$I_{1,2} = \frac{I_0}{2}\left(\sum_{\{r_k\}} \left| \langle\psi_0| \mathcal{M}_{N-1}^{(r_{N-1})} \dots \mathcal{M}_1^{(r_1)} |\psi_0\rangle \right|^2 \pm \mathrm{Re} \sum_{\{r_k\}} e^{i\gamma} \left(\langle\psi_0| \mathcal{M}_{N-1}^{(r_{N-1})} \dots \mathcal{M}_1^{(r_1)} |\psi_0\rangle \right)^2 \right) , \qquad [28]$$

where the second term in the parentheses is the interference term expressible as $\mathrm{Re}\, e^{i\gamma+2i\bar{\chi}_{\rm geom}-\alpha}$ (cf. Eq. (27)). We provide a formal derivation of this result below. This *Gedankenexperiment* to detect the averaged GP could be implemented in a variety of systems, e.g., optical systems with absorptive polarizers or quantum dot detectors in electronic interferometers.

A. Output intensity of the averaged-phase interferometric detector. The observed intensity in the detection scheme presented in Fig. 8 is given by Eq. (28). This result is obtained by analyzing the evolution of the compound system-detector state across the interferometer. The collective state of the particle and all the detectors after the initial beam splitter of the interferometer is $|\Psi_i\rangle = |\psi_0\rangle \otimes [|a = 1\rangle + |a = -1\rangle] \otimes |+...+\rangle / \sqrt{2}$, where $a = \pm 1$ describe the particle being in the upper or lower arm respectively, and $|+...+\rangle$ is the initial state of all the detectors. A "flip" (cf. Fig. 28) applied at the beginning and at the end of the lower arm acts on the system via $R^{-1}(\mathbf{n}_0)\sigma_x^{(s)}R(\mathbf{n}_0)$. The interaction of the system with each of the detectors is described by the Hamiltonian

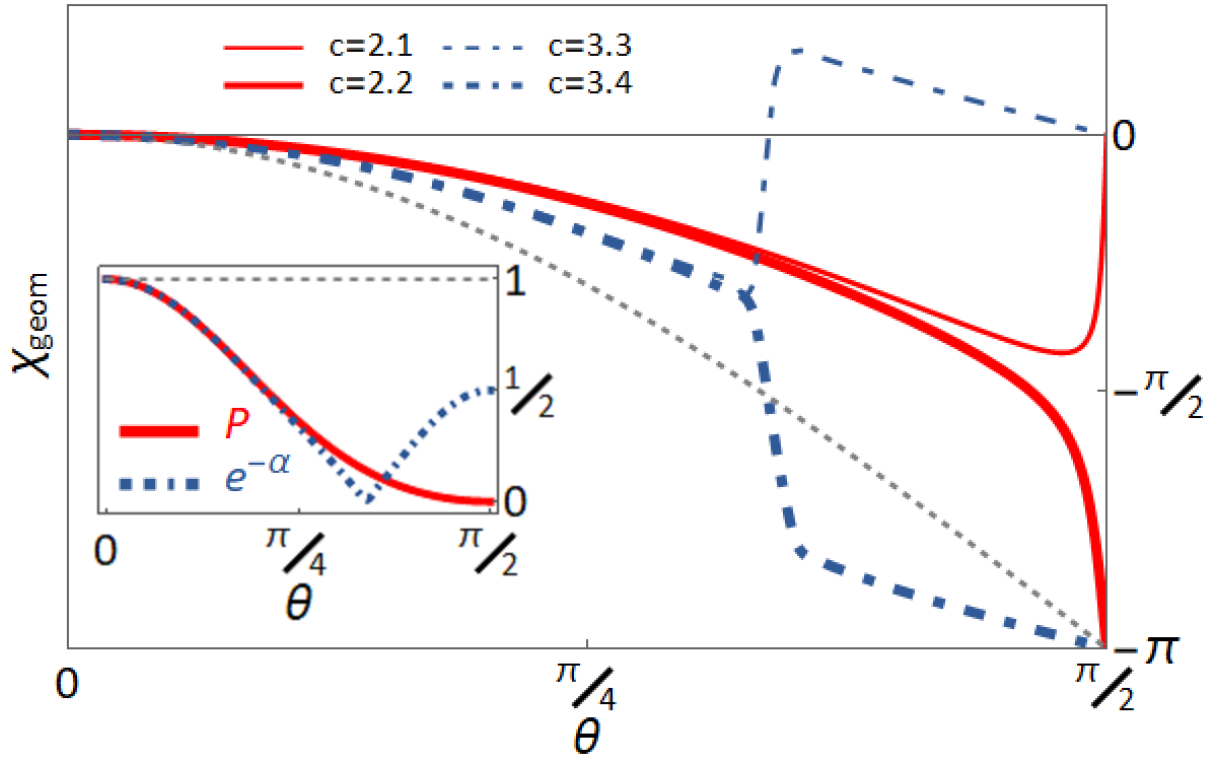

Fig. 7. Non-monotonicity and discontinuity of averaged geometric phases. We show the dependence of the averaged geometric phase on the polar angle θ at different values of the integrated measurement strength (cf. legend) for the averaged geometric phase (blue dot-dashed lines) compared to that of the postselected geometric phase (red solid lines). The ideal strong measurement dependence for $c \to \infty$ is presented as a grey dashed line. The dependence of the averaged GP on θ displays an abrupt transition from monotonic to non-monotonic behavior in the vicinity of $c = 3.35$. The critical strength for the averaged geometric phases differs from that of the postselected geometric phase. The behavior is underlined by the fact that $\chi_{\rm geom}(\theta)$ can assume only discrete values, 0 or $-\pi$, at $\theta = \pi/2$. Inset: The suppression factor $e^{-\alpha}$ (blue dot-dashed line) in the protocol with averaging at $c = 3.3$ compared to the probability of observing the most probable trajectory with postselected readout sequence $\{r_k = +\}$ (red solid line) at $c = 2.1$; the grey dashed line indicates $P = e^{-\alpha} = 1$ for $c \to \infty$, an asymptotic strong measurement. The plots for the protocol with averaging have been obtained by Monte Carlo simulations with $N = 500$ measurement steps per sequence and $N_{\rm realizations} = 500000$ realizations.

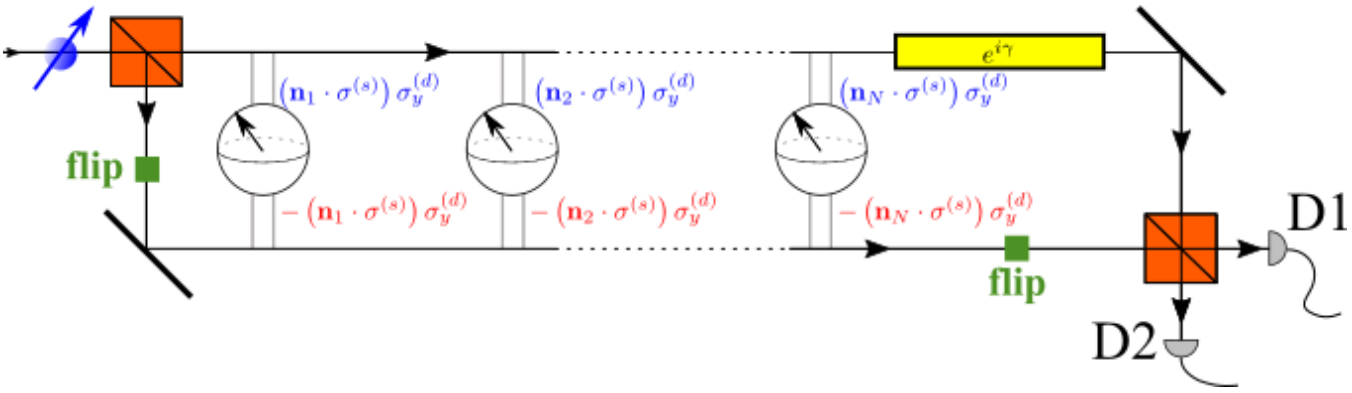

Fig. 8. Experimental setups for observing the averaged measurement induced GPs. Scheme for observing the averaged GP, $\bar{\chi}_{\rm geom}$, in a Mach-Zehnder interference setup. The detectors interact with the particle in both interferometer arms according to different Hamiltonians, $H_{\mathbf{n}}$ and $H_{-\mathbf{n}}$, cf. Eq. (29). Together with the flip of the particle's internal degree of freedom in the lower arm, this ensures that no "which-path" detection takes place, and all readout sequences $\{r_k\}$ contribute to the interference pattern at D1 and D2. For any given readout sequence $\{r_k\}$, the GP accumulated by the particle is opposite in the two arms of the interferometer. We assume an extra phase difference $e^{i\gamma}$ produced by means other than measurements.

$$\tilde{H}_{\mathbf{n}_k} = \lambda(t)[1 - (\mathbf{n}_k \cdot \sigma^{(s)})\sigma_z^{(a)}]\sigma_y^{(d)}/2, \quad [29]$$

where the Pauli z matrix $\sigma_z^{(a)}$ acts on the degree of freedom describing the occupation of the upper and lower arms of the interferometer. The role of $\tilde{H}_{\mathbf{n}_k}$ is to let the detector interact simultaneously with the upper and lower arms via $H_{\mathbf{n}_k}$ and $H_{-\mathbf{n}_k}$, respectively, such that the occupation of one of the two arms is not detected and ensuring that the system in the upper and the lower arms accumulate opposite geometric phases. After the interaction with all the detectors and the action of the final flip (but before the particle passing through the last beam splitter) the global state of the system and detectors reads $\left|\Psi_f\right\rangle = [|\psi_1\rangle\,|a=1\rangle + |\psi_{-1}\rangle\,|a=-1\rangle]/\sqrt{2}$, where $|\psi_1\rangle = \sum_{\{r_k\}} |\{r_k\}\rangle\, \mathcal{M}_N^{(r_N)} \dots \mathcal{M}_1^{(r_1)}\,|\psi_0\rangle\, e^{i\gamma}$ and $|\psi_{-1}\rangle = \sum_{\{r_k\}} |\{r_k\}\rangle\, R^{-1}(\mathbf{n}_0)\sigma_x^{(s)}R(\mathbf{n}_0)\tilde{\mathcal{M}}_N^{(r_N)} \dots \tilde{\mathcal{M}}_1^{(r_1)}R^{-1}(\mathbf{n}_0)\sigma_x^{(s)}R(\mathbf{n}_0)\,|\psi_0\rangle$, where $|\{r_k\}\rangle$ is the state of the collection of detectors the particle interacted with determined by the readout sequence $\{r_k\}$, γ is an extra phase that controls the interference pattern, and the Kraus operators $\mathcal{M}_k^{(r_k)} = M_{\eta_k}(\mathbf{n}_k, r_k) = R^{-1}(\mathbf{n}_k)M_\eta(\mathbf{e}_z, r_k)R(\mathbf{n}_k)$ and $\tilde{\mathcal{M}}_k^{(r_k)} = M_{\eta_k}(-\mathbf{n}_k, r_k) = R^{-1}(\mathbf{n}_k)\sigma_x^{(s)}M_\eta(\mathbf{e}_z, r_k)\sigma_x^{(s)}R(\mathbf{n}_k)$. The intensity of the output signals at D_1 and D_2 are

$$I_{1,2} = I_0 \left\langle \Psi_f \right| (1 \pm \sigma_x^{(a)}) \left| \Psi_f \right\rangle /2.$$

We now employ the fact that the last measurement is projective and postselected to $r_N = +$, with the $r_N = -$ readout not taken into account in calculating $I_{1,2}$. Therefore, $\mathcal{M}_N^{(r_N)} = \mathcal{P}_0 = |\psi_0\rangle\langle\psi_0| = |\mathbf{n}_0\rangle\langle\mathbf{n}_0|$ and $\tilde{\mathcal{M}}_N^{(r_N)} = |-\mathbf{n}_0\rangle\langle-\mathbf{n}_0| = R^{-1}(\mathbf{n}_0)\sigma_x^{(s)}R(\mathbf{n}_0)\,|\mathbf{n}_0\rangle\langle\mathbf{n}_0|\,R^{-1}(\mathbf{n}_0)\sigma_x^{(s)}R(\mathbf{n}_0)$, leading to

$$|\psi_1\rangle = \sum_{\{r_k\}} |\{r_k\}\rangle\,|\psi_0\rangle \times \left(\langle\psi_0|\,\mathcal{M}_{N-1}^{(r_{N-1})} \dots \mathcal{M}_1^{(r_1)}\,|\psi_0\rangle\, e^{i\gamma}\right), \quad [30]$$

$$|\psi_{-1}\rangle = |\sum_{\{r_k\}} |\{r_k\}\rangle\,|\psi_0\rangle \times \left(\langle\psi_0|\,R^{-1}(\mathbf{n}_0)\sigma_x^{(s)}R(\mathbf{n}_0)\tilde{\mathcal{M}}_{N-1}^{(r_{N-1})} \dots \tilde{\mathcal{M}}_1^{(r_1)}R^{-1}(\mathbf{n}_0)\sigma_x^{(s)}R(\mathbf{n}_0)\,|\psi_0\rangle\right). \quad [31]$$

In order to simplify the expression for $|\psi_{-1}\rangle$, we use the property

$$\langle\psi_0|\,R^{-1}(\mathbf{n}_0)\sigma_x^{(s)}R(\mathbf{n}_0)\tilde{\mathcal{M}}_{N-1}^{(r_{N-1})} \dots \tilde{\mathcal{M}}_1^{(r_1)}R^{-1}(\mathbf{n}_0)\sigma_x^{(s)}R(\mathbf{n}_0)\,|\psi_0\rangle = \left(\langle\psi_0|\,\mathcal{M}_{N-1}^{(r_{N-1})} \dots \mathcal{M}_1^{(r_1)}\,|\psi_0\rangle\right)^*, \quad [32]$$

which we prove hereafter. Then, one immediately arrives at Eq. (28) for $I_{1,2}$.

Computation of the phase accumulated through the lower arm. The evolution of the state through the lower arm entering the intensities at the interferometer drain is computed via the property in Eq. (32), which we prove here. We recall from the Methods in the manuscript (cf. Eqs. (19,20) therein) that

$$\delta R = R(\mathbf{n}_{k+1})R^{-1}(\mathbf{n}_k) = \begin{pmatrix} \cos^2\frac{\theta}{2} + e^{-2\pi i/N}\sin^2\frac{\theta}{2} & \frac{1}{2}(1-e^{-2\pi i/N})\sin\theta \\ \frac{1}{2}(1-e^{-2\pi i/N})\sin\theta & \sin^2\frac{\theta}{2} + e^{-2\pi i/N}\cos^2\frac{\theta}{2} \end{pmatrix}, \quad [33]$$

and

$$M_\eta(\mathbf{e}_z, +) = \begin{pmatrix} 1 & 0 \\ 0 & \sqrt{1-\eta} \end{pmatrix}, \; M_\eta(\mathbf{e}_z, -) = \begin{pmatrix} 0 & 0 \\ 0 & \sqrt{\eta} \end{pmatrix}. \quad [34]$$

Using the hermiticity of $M_\eta(\mathbf{e}_z, r_k)$, and the identities

$$\sigma_x^{(s)}\delta R\sigma_x^{(s)} = e^{-2\pi i/N}\sigma_z^{(s)}\delta R^{-1}\sigma_z^{(s)} = e^{-2\pi i/N}\sigma_z^{(s)}\delta R^\dagger\sigma_z^{(s)}, \quad [35]$$

$$\sigma_z^{(s)}M_\eta(\mathbf{e}_z, r_k)\sigma_z^{(s)} = M_\eta(\mathbf{e}_z, r_k), \quad [36]$$

for δR, we can write

$$\begin{aligned} &\langle\psi_0|\,R^{-1}(\mathbf{n}_0)\sigma_x^{(s)}R(\mathbf{n}_0)\tilde{\mathcal{M}}_{N-1}^{(r_{N-1})} \dots \tilde{\mathcal{M}}_1^{(r_1)}R^{-1}(\mathbf{n}_0)\sigma_x^{(s)}R(\mathbf{n}_0)\,|\psi_0\rangle \\ &\quad = \langle\mathbf{e}_z|\,\sigma_x^{(s)}\delta R\sigma_x^{(s)}M_\eta(\mathbf{e}_z, r_{N-1})\sigma_x^{(s)}\delta R\sigma_x^{(s)}M_\eta(\mathbf{e}_z, r_{N-2})\sigma_x^{(s)}\delta R \dots \delta R\sigma_x^{(s)}M_\eta(\mathbf{e}_z, r_1)\sigma_x^{(s)}\delta R\sigma_x^{(s)}\,|\mathbf{e}_z\rangle \\ &\quad = e^{-2\pi i N/N}\,\langle\mathbf{e}_z|\,\sigma_z^{(s)}\delta R^\dagger\sigma_z^{(s)}M_\eta(\mathbf{e}_z, r_{N-1})\sigma_z^{(s)}\delta R^\dagger \dots \delta R^\dagger\sigma_z^{(s)}M_\eta(\mathbf{e}_z, r_1)\sigma_z^{(s)}\delta R^\dagger\sigma_z^{(s)}\,|\mathbf{e}_z\rangle \\ &\quad = \langle\mathbf{e}_z|\,\delta R^\dagger M_\eta(\mathbf{e}_z, r_{N-1})\delta R^\dagger M_\eta(\mathbf{e}_z, r_{N-2})\delta R^\dagger \dots \delta R^\dagger M_\eta(\mathbf{e}_z, r_1)\delta R^\dagger\,|\mathbf{e}_z\rangle \\ &\quad = (\langle\mathbf{e}_z|\,\delta R M_\eta(\mathbf{e}_z, r_1)\delta R M_\eta(\mathbf{e}_z, r_2)\delta R \dots \delta R M_\eta(\mathbf{e}_z, r_{N-1})\delta R\,|\mathbf{e}_z\rangle)^*. \end{aligned} \quad [37]$$

Using the explicit representation of

$$|\mathbf{e}_z\rangle = \begin{pmatrix} 1 \\ 0 \end{pmatrix}, \quad [38]$$

(cf. Eq. (14) in the manuscript), we consider

$$\begin{aligned} &\langle\mathbf{e}_z|\,\delta R M_\eta(\mathbf{e}_z, r_1)\delta R M_\eta(\mathbf{e}_z, r_2)\delta R \dots \delta R M_\eta(\mathbf{e}_z, r_{N-1})\delta R\,|\mathbf{e}_z\rangle \\ &\quad = (\langle\mathbf{e}_z|\,\delta R M_\eta(\mathbf{e}_z, r_1)\delta R M_\eta(\mathbf{e}_z, r_2)\delta R \dots \delta R M_\eta(\mathbf{e}_z, r_{N-1})\delta R\,|\mathbf{e}_z\rangle)^T \\ &\quad = \langle\mathbf{e}_z|\,\delta R M_\eta(\mathbf{e}_z, r_{N-1})\delta R M_\eta(\mathbf{e}_z, r_{N-2})\delta R \dots \delta R M_\eta(\mathbf{e}_z, r_1)\delta R\,|\mathbf{e}_z\rangle, \end{aligned} \quad [39]$$

where T denotes transposition, and in the last step we used $\delta R^T = \delta R$ and $M_\eta(\mathbf{e}_z, r)^T = M_\eta(\mathbf{e}_z, r)$, cf. (33, 34). Finally, noticing that

$$\langle\mathbf{e}_z|\,\delta R M_\eta(\mathbf{e}_z, r_{N-1})\delta R M_\eta(\mathbf{e}_z, r_{N-2})\delta R \dots \delta R M_\eta(\mathbf{e}_z, r_1)\delta R\,|\mathbf{e}_z\rangle = \langle\psi_0|\,\mathcal{M}_{N-1}^{(r_{N-1})} \dots \mathcal{M}_1^{(r_1)}\,|\psi_0\rangle, \quad [40]$$

one obtains Eq. (32), as desired.